Cucurbitacin IIa promotes the immunogenic cell death-inducing effect of doxorubicin and modulates immune microenvironment in liver cancer

SUJUAN LI[1-3*], SEN WANG[1-3*], ANPING ZHANG[1-3], LIXIA LUO[1-3], JIE SONG[1-3], GUOLI WEI[1-3] and ZHIJUN FANG[1,3]

[1]Affiliated Hospital of Integrated Traditional Chinese and Western Medicine, Nanjing University of Chinese Medicine, Nanjing, Jiangsu 210023; [2]Department of Oncology, Nanjing Lishui District Hospital of Traditional Chinese Medicine, Nanjing, Jiangsu 211200; [3]Jiangsu Province Academy of Traditional Chinese Medicine, Nanjing, Jiangsu 210028, P.R. China

Received November 1, 2023; Accepted February 1, 2024

DOI: 10.3892/ijo.2024.5625

Abstract. The immunogenic cell death (ICD) has aroused great interest in cancer immunotherapy. Doxorubicin (DOX), which can induce ICD, is a widely used chemotherapeutic drug in liver cancer. However, DOX-induced ICD is not potent enough to initiate a satisfactory immune response. Cucurbitacin IIa (CUIIa), a tetracyclic triterpene, is a biologically active compound present in the *Cucurbitaceae* family. The present study assessed the effects of the combination of DOX and CUIIa on the viability, colony formation, apoptosis and cell cycle of HepG2 cells. *In vivo* anticancer effect was performed in mice bearing H22 tumor xenografts. The hallmark expression of ICD was tested using immunofluorescence and an ATP assay kit. The immune microenvironment was analyzed using flow cytometry. The combination of CUIIa and DOX displayed potent apoptosis inducing, cell cycle arresting and *in vivo* anticancer effects, along with attenuated cardiotoxicity in H22 mice. The combination of DOX and CUIIa also facilitated ICD as manifested by elevated high-mobility group box 1, calreticulin and ATP secretion. This combination provoked a stronger immune response in H22 mice, including dendritic cell activation, increment of cytotoxic T cells and T helper 1 cells. Moreover, the proportion of immunosuppressive cells including myeloid-derived suppressor cells, T regulatory cells and M2-polarized macrophages, decreased. These data suggested that CUIIa is a promising combination partner with DOX for liver cancer treatment, probably via triggering ICD and remolding the immune microenvironment.

Correspondence to: Professor Guoli Wei or Professor Zhijun Fang, Jiangsu Province Academy of Traditional Chinese Medicine, 100 Shizi Street, Nanjing, Jiangsu 210028, P.R. China
E-mail: weiguoli@jsatcm.com
E-mail: fangzhijun@jsatcm.com

*Contributed equally

Abbreviations: CI, combination index; CRT, calreticulin; CTLs, cytotoxic T lymphocytes; CUIIa, cucurbitacin IIa; DCs, dendritic cells; DOX, doxorubicin; HMGB1, high-mobility group box 1; ICD, immunogenic cell death; MDSCs, myeloid-derived suppressor cells; TAM, tumor-associated macrophages; TH1, T helper 1 cells; Treg, regulatory T cells; TME, tumor microenvironment

Key words: CUIIa, DOX, ICD, TME, liver cancer

Introduction

The liver, the largest internal organ in humans, plays a vital role in the organism's physical function (1,2). Currently, chemotherapy remains the primary treatment option for liver cancer (3). However, the benefits of chemotherapy are highly limited in patients with tumor metastasis, tumor recurrence, multi-drug resistance or toxic side effects (4).

Immunosuppressive immune cells assemble in the liver cancer microenvironment and are associated with a poor prognosis. Immunogenic cell death (ICD) has provoked extensive interest in the field of cancer immunotherapy, and several clinical studies have shown that some chemotherapy agents induce ICD (5). Doxorubicin (DOX), is a broad-spectrum antineoplastic agent that induces ICD (6-9). DOX has been confirmed to effectively inhibit the topoisomerase IIα-mediated DNA replication by the intercalation into nuclear DNA strands in cancer cells (10,11). ICD is characteristic of danger-associated molecular patterns (DAMP), such as exposure to calreticulin (CRT) on the cell surface, the release of high-mobility group box 1 (HMGB1) and secretion of ATP, which recruits innate immune cells such as dendritic cells (DCs), and then triggers tumor specific immune responses such as cytotoxic T lymphocytes (CTLs) to eliminate residual cancer cells (12,13). However, ICD is typically limited by the intrinsic immunosuppressive tumor microenvironment (TME) (14), including regulatory T (Treg) cells, myeloid-derived suppressor cells (MDSCs) and tumor-associated macrophages (TAMs). These immunosuppressive cells in the TME directly or indirectly suppress effector cells by inhibiting DCs differentiation, migration and antigen presentation (15). The degree of functional

impairment of CTLs and other immunocompetent cells is closely related to the prognosis of cancer (16). In addition, CTLs dysfunction reduces the effect of ICD.

However, studies have revealed that DOX alone cannot induce sufficient ICD to initiate a satisfactory anticancer immune response by itself (17,18). Therefore, the combination of Chinese herbs and DOX to enhance the effect of ICD has become a research focus. A previous study demonstrated that the combination of low-dose icaritin and DOX exhibited a synergistic effect on ICD induction (19). Wu *et al* (18) found that ginsenoside Rg3 nanoparticles strengthened the DOX-induced ICD effect. These studies indicated that it is feasible to enhance the ICD effect by combining traditional Chinese medicine with DOX.

Cucurbitacin IIa (CUIIa) is a biologically active tetracyclic triterpenoid found in *Cucurbitaceae*. CUIIa has attracted considerable attention because of its anti-inflammatory and antiviral properties (20,21). Although the anticancer mechanisms of several cucurbitacins have been elucidated, the anticancer activity is rarely been reported. Studies have demonstrated that CUIIa induces cell cycle arrest, and inhibits the proliferation and migration of tumor cells in prostate, lung and liver cancer (22-25). CUIIa was found to induce caspase-3-dependent apoptosis, whereas ICD was caspase-dependent. However, whether CUIIa regulates the ICD requires further investigation.

In the present study, it was demonstrated that the combination of CUIIa and DOX activated ICD biomarkers in liver cancer, and induced an effective immune response. These findings provided a promising approach to assist tumor chemoimmunotherapy against liver cancer.

Materials and methods

Cells and reagents. The human liver cancer cell lines HepG2 and Hep3B cells and the mouse liver cancer cell line H22 cells were cultured in DMEM medium containing 10% v/v FBS (Gibco; Thermo Fisher Scientific, Inc.), as well as 100 mg/ml of streptomycin and 100 units/ml penicillin at 37˚C in a humidified environment with 5% CO_2 supply. DOX hydrochloride was obtained from Zhejiang Hisun pharmaceutical Co., Ltd. CUIIa (cat. no. HAO62805198) was purchased from Baoji Herbest Bio-Tech Co., Ltd. 4',6-diamidino-2-phenylindole (DAPI) was obtained from Shanghai Aladdin Biochemical Technology Co., Ltd. CD31 (cat. no. ab28364), Ki-67 (cat. no. ab15580), CRT (cat. no. ab92516), Caspase-3 (cat. no. ab184787) and HMGB1 (cat. no. ab79823) antibodies were all obtained from Abcam.

MTT assay. The *in vitro* cytotoxicity of CUIIa and DOX was determined using MTT assay. HepG2 and Hep3B cells ($1x10^4$ per well) were seeded within 96-well plates, respectively. Subsequently, CUIIa and DOX (concentration=0.6, 1.8, 5.4, 16.2 and 48.6 μM) was added to cells for 24-h incubation. Cells were then added with MTT reagent (5 mg/ml in PBS) at 37˚C for 4 h, and the purple precipitate was dissolved by DMSO (200 μl) before measurement at 570 nm. IC_{50} was calculated using the GraphPad Prism software.

Colony formation. Colony formation assay was initiated by seeding cells in 6-well plates. HepG2 and Hep3B cells (2,000 cells per well) were seeded within 6-well plates for 6 days. The colony is defined to consist of at least 50 cells. Then, the colony-forming cells were treated with drugs at indicated concentration for another 4 days. At the end, the cells were fixed with 4% paraformaldehyde for 30 min and stained with 0.1% crystal violet for 20 min at room temperature. The number of colonies was quantified by ImageJ software (version 1.53f; National Institutes of Health).

Apoptosis detection and cell cycle analysis. HepG2 and Hep3B cells ($2x10^5$ per well) were seeded within 6-well plates and treated with drugs at indicated concentrations for 24 h. The apoptotic ratio was determined by flow cytometry using Annexin V Apoptosis Detection kit (cat. no. AT101C), which was obtained from MultiSciences Biotech Co., Ltd. The cell cycle was determined by flow cytometry using the cell cycle analysis kit. Experimental data were analyzed by FlowJo and GraphPad Prism software.

Immunofluorescence staining. HepG2 cells ($5x10^4$ per well) were seeded within 24-well plates and treated with drugs at indicated concentrations for 24 h. Afterwards, cells were fixed with 4% paraformaldehyde for 20 min, and washed three times in PBS. The cells were incubated in blocking buffer [1% (w/v) BSA (Gibco; Thermo Fisher Scientific, Inc.) in PBS] for 30 min and subsequently incubated overnight at 4˚C with primary antibodies (HMGB1 or CRT) diluted (1:1,500) in the blocking buffer. The sample was washed three times in PBS and incubated overnight at 4˚C with secondary antibodies in the blocking buffer. The nuclei were counterstained with DAPI (5 μg/ml).

Hoechst 33342 staining. The apoptosis detection was evaluated by Hoechst 33342 staining assay kit (cat. No. P0133), which was obtained from Beyotime Institute of Biotechnology. After 24 h incubation with DOX or/and CUIIa, cells were further stained with Hoechst 33342 for 15 min at 37˚C. Then the stained cells were observed under a fluorescence microscope.

ATP release assay. After 24 h incubation with DOX or/and CUIIa, extracellular ATP level of HepG2 cells was detected with an ATP Assay Kit (cat. no. S0026; Beyotime Institute of Biotechnology) by employing firefly luciferase-catalyzed oxidation of D-luciferin to produce light in the presence of ATP. The fluorescence was detected with the multiscan spectrum (Synergy H1; BioTek Instruments, Inc.).

Animal study. In total, 45 specific pathogen-free male ICR mice (age, 4 weeks-old; weight, 18-22 g) were purchased from Shanghai SLAC Laboratory Animal Co., Ltd. (Shanghai, China). Mice were housed in a specific pathogen-free environment at a constant temperature of 22±1˚C and 55±5% humidity, and provided with standard laboratory diet and drinking water ad libitum in a 12/12-h dark/light cycle. The mouse liver cancer cell line H22 cells were cultured in DMEM medium, and $1x10^7$ cells in PBS (500 μl) were injected into the abdominal cavity of each mouse. After seven days, the mice were sacrificed and ascites were collected, then diluted with PBS, and subcutaneously injected into the right flank of mice. After three days, the mice were then randomly divided into 4 groups, including the control group (0.9% NaCl solution)

and CUIIa groups (30, 60 and 90 mg/kg). Mice in CUIIa groups were gavaged once a day, and all the mice were sacrificed at day 12. For the anticancer study of CUIIa and DOX combination, mice were then randomly divided into 4 groups, including the control group, CUIIa group (90 mg/kg), DOX group (3 mg/kg) and the combined group. DOX was injected intravenously once every 3 days. Mice in CUIIa groups were gavaged once a day, and all the mice were sacrificed at day 12. At experimental endpoint, all mice were euthanized by intravenous injection of pentobarbital sodium.

Hematoxylin-eosin staining (H&E) and immunohistochemical staining. All tumor tissues were fixed in 10% neutral formalin for 48 h at room temperature, embedded in paraffin wax, and cut into 4-μm thick serial sections. Tissue slices (heart, liver, spleen, lung and kidney) were stained with H&E to assess the toxicity of drugs. And tumor tissues were stained immunohistochemically with primary anti-Ki-67 (1:1,000), Caspase-3 (1:1,500) and CD31 (1:2,000) antibodies according to the manufacturers' instructions. In details, tissue sections were deparaffinized in xylene and ethanol series (anhydrous ethanol, 95% alcohol, 95% alcohol, and 80% alcohol) and subjected to antigen retrieval in citrate buffer. The sections were incubated with primary antibodies overnight at 4˚C. The secondary antibody against HRP-conjugated Goat Anti-Rabbit IgG (1:1,000) was obtained from Abcam (cat. no. ab6721) and incubated at room temperature for 50 min. The sections were further stained with DAB and hematoxylin. The expression of Ki67, Caspase-3 and CD31 was observed under a light microscope (Nikon Corporation).

Enzyme-linked immunosorbent assay (ELISA). The levels of TNF-α, IFN-γ, IL-12, IL-4, IL-10 and CCL2 in the homogenate supernatant of tumor tissue were evaluated by ELISA kits according to the manufacturer's instructions. TNF-α (cat. no. E-MSEL-M0002), IFN-γ (cat. no. E-MSEL-M0007), IL-12 (cat. no. E-MSEL-M0004), IL-4 (cat. no. E-MSEL-M0008), IL-10 (cat. no. E-MSEL-M0031) and CCL2 (cat. no. E-EL-M3001) ELISA kits were purchased from Elabscience Biotechnology Co. Ltd.

Evaluation of immune cells in mice bearing H22 xenografts by flow cytometry. Tumor-draining lymph nodes and spleens from mice bearing H22 tumor were harvested and processed into single cell suspensions through a 200-mesh sterile filter. Spleen was then treated with ACK lysis buffer to remove red blood cells. Anti-mouse CD16/32 Fc receptor block antibody (BioLegend, Inc.) were used to block the non-specific antibody binding. To evaluate the antigen presentation ability of DCs cells, single cell suspensions were stained with Fixable Viability Dye eFluor 780 (eBioscience; Thermo Fisher Scientific, Inc.), anti-CD11c-APC, anti-CD80-PE, anti-CD86-BV421 and anti-MHCII-FITC antibodies or an isotype IgG control (BioLegend, Inc.) according to the manufacturers' instruction. Samples were collected on BD FACS Verse Flow Cytometer (BD Biosciences), and data were analyzed using FlowJo V.10.1 software (Tree Star, Inc.).

To assess the abundance of CTLs ($CD4^-CD8^+IFN\text{-}\gamma^+$) and TH1 cells ($CD4^+CD8^-IFN\text{-}\gamma^+$), single cell suspensions were stained with Fixable Viability Dye eFluor™ 780 (eBioscience; Thermo Fisher Scientific, Inc.), anti-CD3-PE cy7, anti-CD4-APC, anti-CD8-FITC, and anti-IFN-γ-PE antibodies (BioLegend, Inc.). For intracellular cytokine staining, $1x10^6$ cells were stimulated with complete RPMI-1640 containing activation cocktail and brefeldin A for 6 h (BioLegend, Inc.). For analysis of Treg cells, the antibodies used included APC-labeled anti-mouse CD4 antibody, PE cy7-labeled anti-mouse CD3 antibody and PE-labeled anti-mouse Foxp3 antibody (18).

For analysis of M1/M2 macrophages, the acquired suspended cells were stained with anti-Gr1-PE, anti-F4/80-APC, anti-MHCII-FITC and anti-CD206-PE-Cy7 antibodies (BioLegend, Inc.). Cells were stained with anti-CD11b-APC and anti-Gr-1-PE antibodies (BioLegend, Inc.) to examine the ratio of MDSCs. Moreover, cells were stained with anti-CD11b-FITC, anti-Ly6G-PE, anti-Ly6C-Cy5 antibodies (BioLegend, Inc.) to detect the proportion of M-MDSCs.

Statistical analyses. All experiments were performed at least three times. All data were analyzed using GraphPad Prism 8.0 (Dotmatics) by unpaired Student's t-test and one-way analysis of variance (ANOVA) with Bonferroni correction. Data were presented as the mean ± SD. $^*P<0.05$ was considered to indicate a statistically significant difference.

Results

CUIIa suppresses liver cancer tumor growth. The MTT assay was used to evaluate the inhibitory effect of CUIIa on the proliferation of liver cancer cells. The results revealed that the inhibitory potential of CUIIa depended on its concentration, and a more powerful effect was achieved by CUIIa at a higher concentration. IC_{50} of CUIIa on HepG2 and Hep3B cells were 31.5 and 28.1 μM, respectively (Fig. 1A). Therefore, the concentration of 30 μM was selected for subsequent experiments. CUIIa almost blocked the colony formation in both HepG2 and Hep3B cells (Fig. 1B). As demonstrated in Fig. 1C, CUIIa clearly promoted the apoptosis in both HepG2 and Hep3B cells, and the apoptotic rate increased to 41.9 and 26.00%, respectively. Cell cycle analysis by flow cytometry revealed that CUIIa significantly decreased the percentage of cells in the G0/G1 phase and S phases and increased the percentage of cells in the G2/M phase (Fig. 1D). These results suggested that CUIIa might inhibit liver cancer cells growth by maintaining cells in the G2/M phase.

Next, the anticancer effect of CUIIa on H22 cells-bearing mice was examined. Most mice in the control group were in poor health, and became lethargic, listless and indulged in sleep. Fur withered as tumor size increased. The tumor growth curves of H22 xenografts are depicted in Fig. 1E. The average volume was 651.53 mm^3 in CUIIa low-dose group and 513.66 mm^3 in CUIIa medium-dose group. The average tumor volume in the CUIIa high-dose group was 453.76 mm^3, significantly smaller than that of the control group (998.02 mm^3) at day 11. In addition, no pathological changes were observed in the major organs (heart, liver, spleen, lungs and kidneys) of the control and high-dose CUIIa groups by H&E staining (Fig. 1F).

CUIIa promotes the anticancer effect of DOX in vitro. Dox is widely used in liver cancer chemotherapy treatment. However,

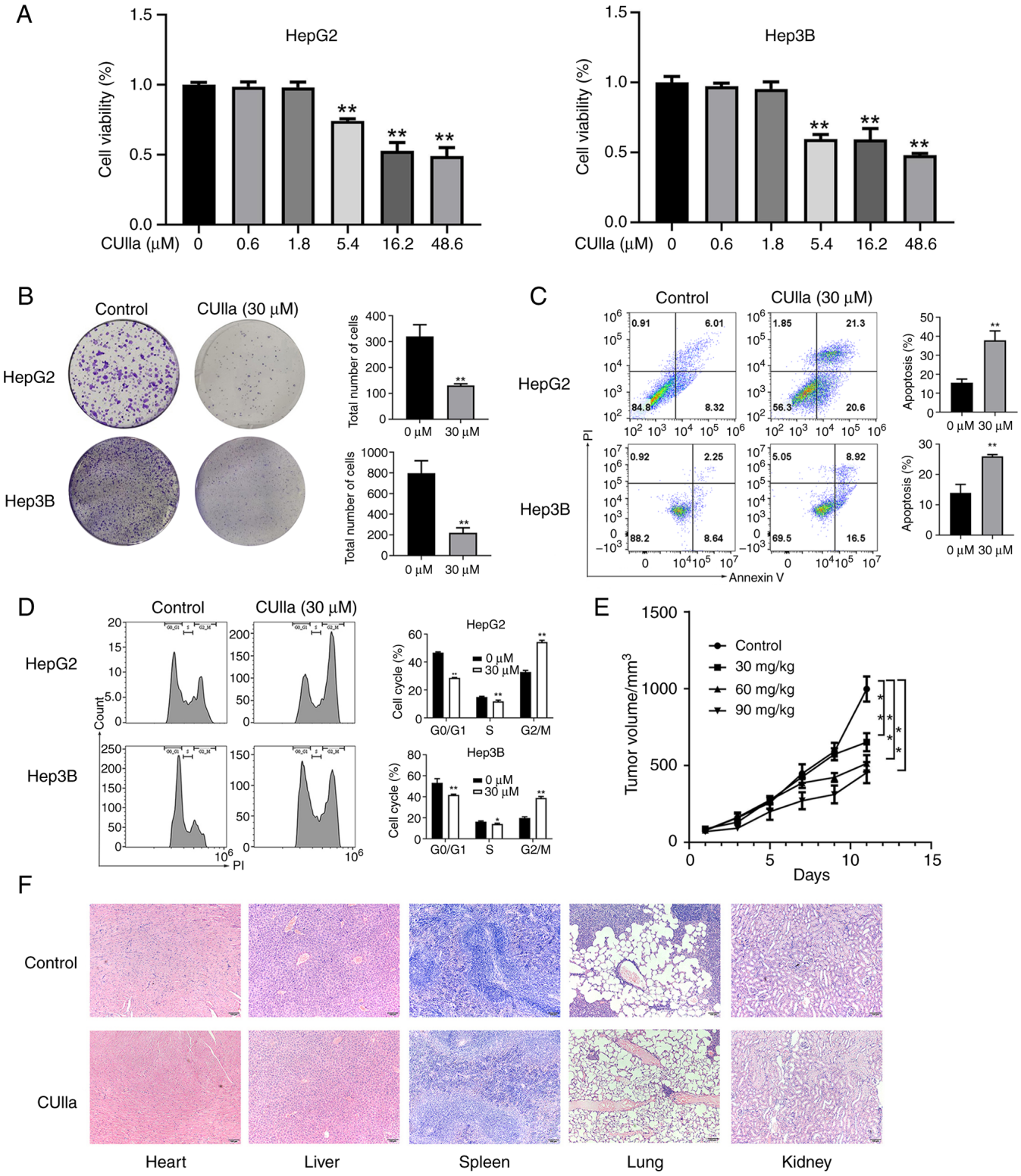

Figure 1. The inhibitory effects of CUIIa on liver cancer *in vitro* and *in vivo*. (A) Viability of HepG2 and Hep3B cells after 24 h exposure to CUIIa. (B) Colony formation of HepG2 and Hep3B treated with CUIIa (30 μM). (C) Apoptosis and (D) cell cycle of HepG2 and Hep3B cells after 24 h CUIIa exposure (30 μM). (E) Tumor volume of mice bearing H22 xenografts. (F) H&E staining of major organs from H22 mice in the CUIIa group (90 mg/kg). Scale bar, 100 μm. Data are presented as the mean ± SD. *P<0.05 and **P<0.01. CUIIa, cucurbitacin IIa.

DOX-induced cardiotoxicity greatly limits its clinical therapeutic utility (26). In the present study, it was examined whether CUIIa strengthened the anticancer effect of DOX and lowered cardiotoxicity. As revealed in Fig. 2A, CUIIa promoted DOX cytotoxicity in HepG2 cells. The combination index (CI) was used to evaluate the combined effect of DOX plus CUIIa (27), namely, synergistic (CI<1), additive (CI=1) or antagonistic (CI>1) effects (28). The IC_{50} of DOX monotherapy was 1.1 μM for HepG2 cells, while the IC_{50} of CUIIa monotherapy was 31.5 μM. When used in combination, the inhibition rate

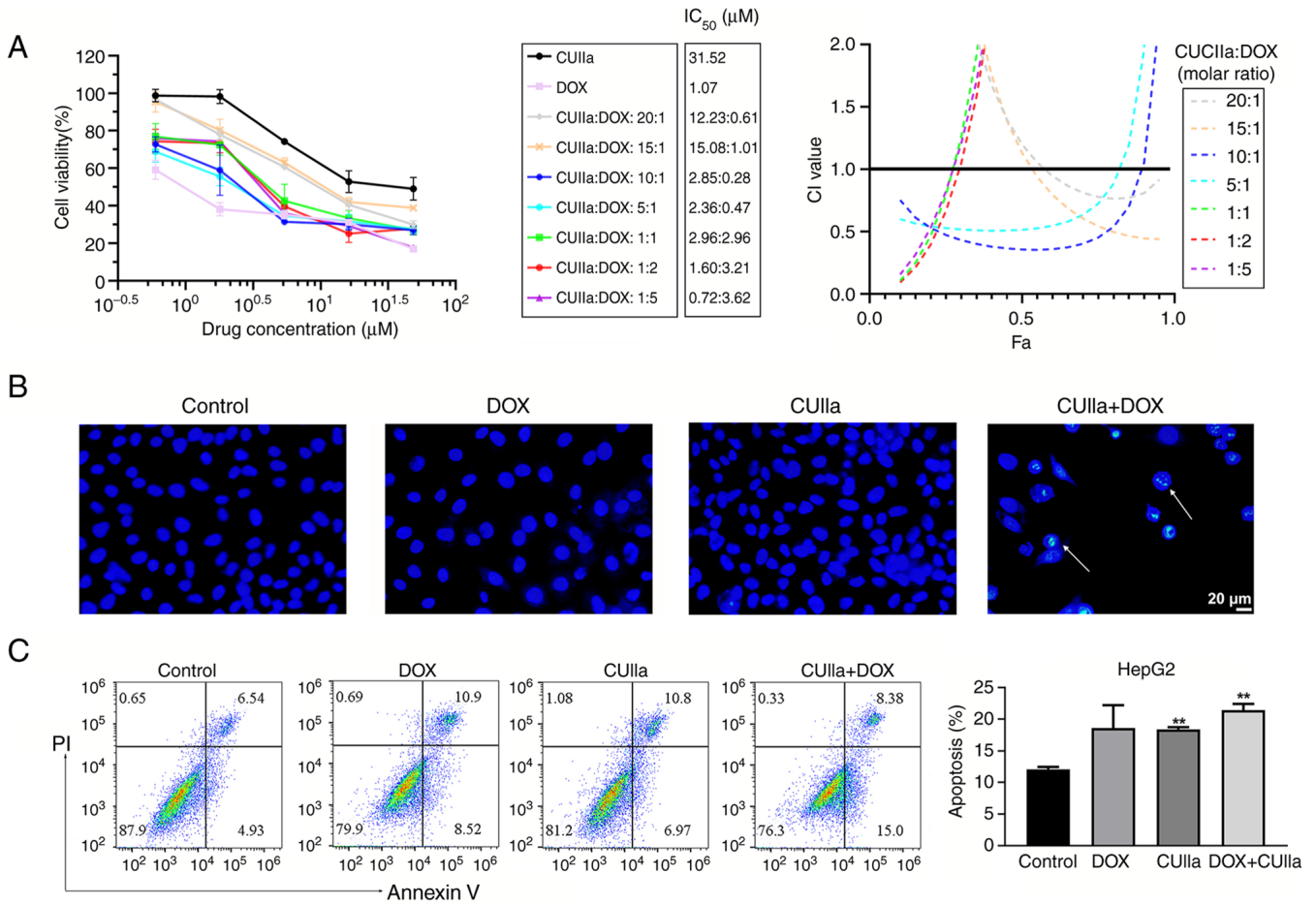

Figure 2. Combination of CUIIa and DOX suppresses viability and induces apoptosis in HepG2 cells *in vitro*. (A) Viability of HepG2 cells treated DOX with/or CUIIa at different molar ratio and the corresponding CI vs. Fa plots. (B) Hoechst staining of HepG2 cells (white arrows indicating apoptosis). (C) Apoptosis of HepG2 cells treated with DOX (0.29 μM), CUIIa (2.86 μM) or their combination by flow cytometry. Data are presented as the mean ± SD. **P<0.01. CUIIa, cucurbitacin IIa; DOX, doxorubicin; CI, combination index.

reached 50% in CUIIa (2.85 μM) plus DOX (0.28 μM) group (10:1 ratio), and meanwhile the calculated CI was equal to 0.36 (Fig. 2A). Low doses with a pleasant treatment efficacy shall reduce the side effects of DOX. Therefore, the concentration of CUIIa (2.86 μM) plus DOX (0.29 μM) was chosen for the following *in vitro* study.

Hoechst staining and flow cytometry verified that this combination induced apoptosis in HepG2 cells. As demonstrated in Fig. 2B, the majority of nuclei in the control, CUIIa and DOX groups exhibited round and uniform light blue fluorescence, whereas apoptotic nuclear staining in the combination group was enhanced, and the fluorescence was brighter. The structures were either condensed or clumpy. Moreover, the number of cells in the field of vision was significantly reduced in the combination group. Accordingly, FITC-annexin V-PI flow cytometry identified a significantly higher rate of apoptosis in the combination group compared with the control group (Fig. 2C).

Combination of CUIIa and DOX displays potent inhibitory effect on H22 tumor growth. After confirming the anticancer effect of the combination *in vitro*, it was further examined the anticancer effect *in vivo*. A significant reduction in the tumor volume was observed after the application of combination therapy to mice with subcutaneous tumors *in vivo* (Fig. 3A and C). H&E staining revealed necrosis, vacuolar cardiomyocyte and inflammatory cells in DOX-treated tumor-bearing mice, consistent with a previous study (29). After the combinatory treatment, the pathological status of heart was improved obviously (Fig. 3B). Therefore, CUIIa ameliorated DOX-induced myocardial toxicity. No body weight loss was observed in any of the treated groups (Fig. 3D). The combination therapy significantly promoted the level of immuno-stimulatory cytokines (TNF-α, IFN-γ and IL-12) and inhibited the secretion of the immunosuppressive cytokines (IL-4, IL-10 and CCL2) in tumor tissues (Fig. 3E). H&E staining was also used to observe the morphology of the tumor tissue in each group and evaluate the therapeutic effect of the combinatory treatment (Fig. 3F). The tumor cells in the control group were densely arranged with a high nuclear-to-cytoplasmic ratio. In both DOX group and CUIIa group, cells and nuclei were more irregular in shape with a low nuclear to cytoplasmic ratio. The combination group had the lowest nuclear-to-cytoplasmic ratio among the four groups. The cells were thinly arranged and the cytoplasm was broken and dissolved. To further investigate the proliferation and apoptosis of tumor cells, the expression of the proliferation marker Ki67, the apoptosis marker Caspase-3

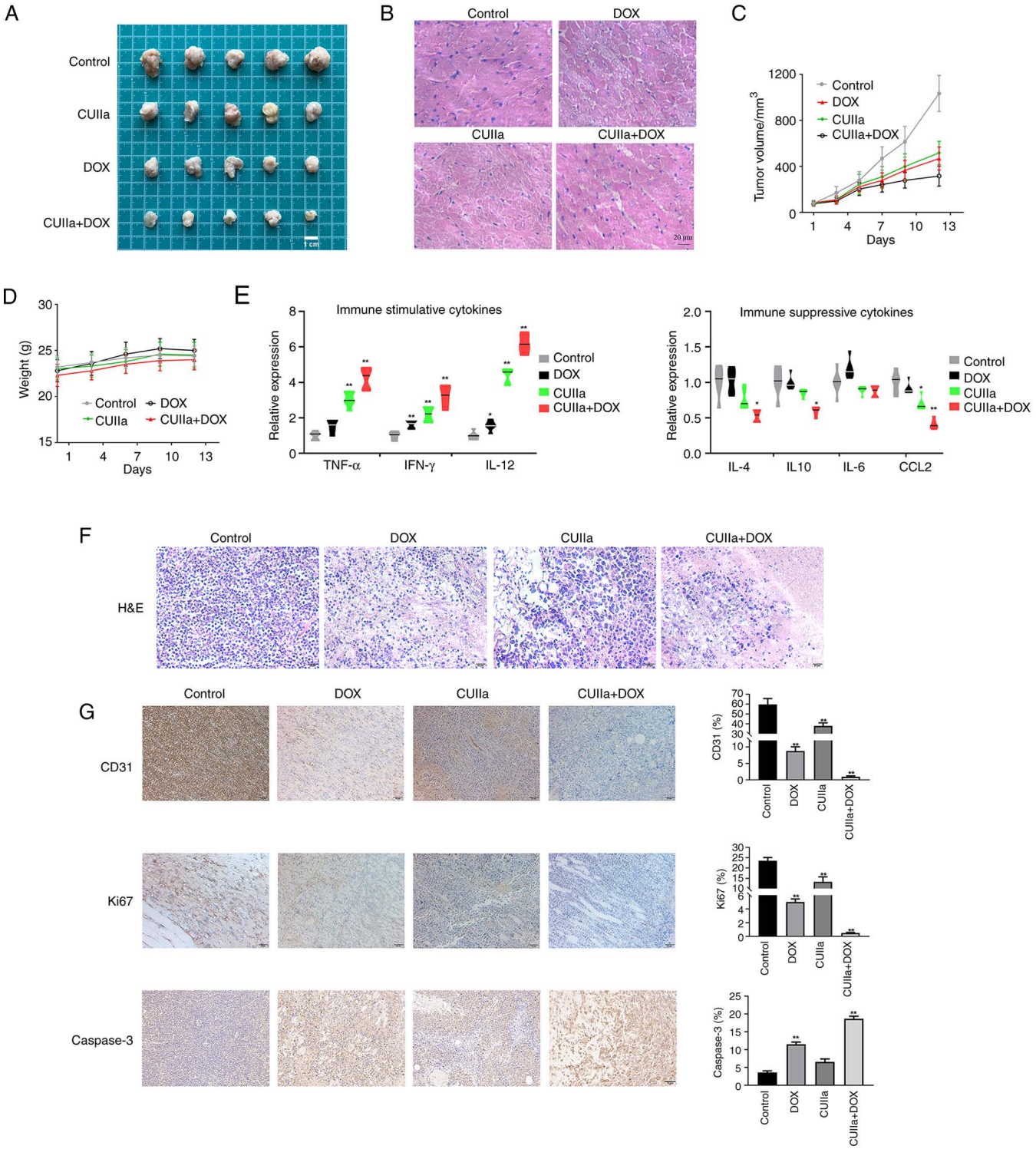

Figure 3. Combination of CUIIa and DOX represses tumor growth of H22-bearing mice. (A) Representative tumors of mice in each group 12 days after treatment. (B) H&E staining of heart in mice. (C) Tumor volume and (D) weight of mice in each group. (E) The level of immuno-stimulatory cytokines (TNF-α, IFN-γ and IL-12) and immunosuppressive cytokines (IL-4, IL-10, IL-6 and CCL2) in tumor tissues. (F) H&E staining of tumor sections. Scale bar, 20 μm. (G) Ki67, Caspase-3 and CD31 expression in tumor sections. Scale bar, 50 μm. Data are presented as the mean ± SD. *P<0.05 and **P<0.01. CUIIa, cucurbitacin IIa; DOX, doxorubicin.

and the endovascular epithelial marker CD31 in xenograft tumors was evaluated by immunohistochemistry (Fig. 3G). The results revealed that combination therapy inhibited tumor growth as well as the expression of Ki67 and CD31 in H22 mice, and meanwhile promoted the expression of Caspase-3.

CUIIa strengthens the ICD induced by DOX. Exposure of CRT on the cell membrane as well as the release of ATP and HMGB1 into the extracellular compartment occur during ICD (30). Immunofluorescence staining demonstrated that the combination of CUIIa and DOX induced a strong ICD response in HepG2 cells, as evidenced by enhanced CRT

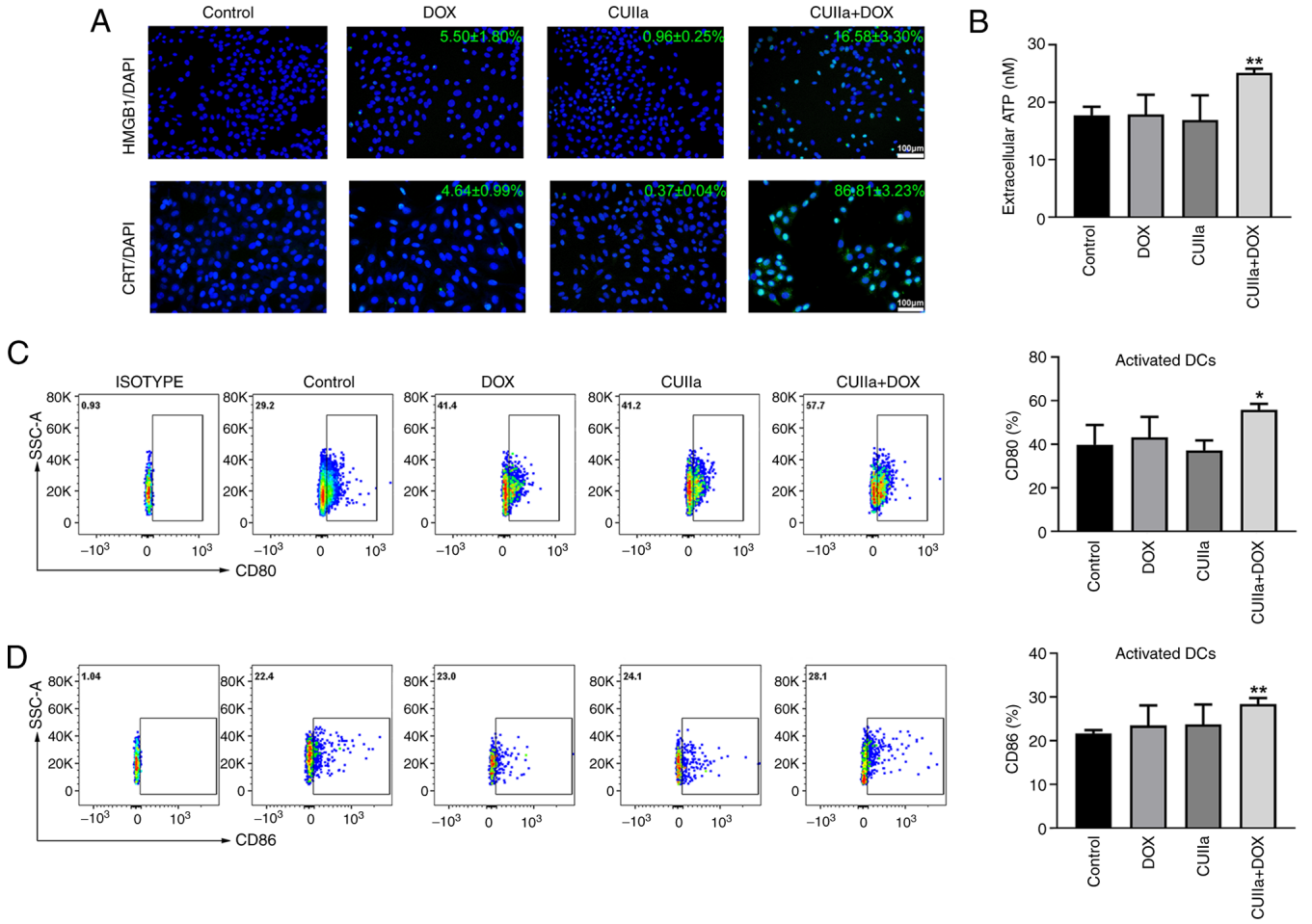

Figure 4. Combination of CUIIa and DOX induces immunogenic cell death. (A) Immunofluorescence assays of HMGB1 and CRT expression in HepG2 cells. (B) Extracellular ATP levels in HepG2 cells. (C and D) Activation of DCs in the (C) spleen and (D) lymph nodes from H22 mice was measured by flow cytometry. Data are presented as the mean ± SD. *P<0.05 and **P<0.01. CUIIa, cucurbitacin IIa; DOX, doxorubicin; DCs, dendritic cells; HMGB1, high-mobility group box 1; CRT, calreticulin.

exposure and HMGB1 release from tumor cells, which are key biomarkers of ICD (Fig. 4A). In addition, the combination of CUIIa and DOX significantly promoted the secretion of ATP into the extracellular compartment of HepG2 cells (Fig. 4B).

DCs play a key role in initiating immune responses and maintaining immune tolerance (31). Activation of DCs is an important part of ICD. Flow cytometry showed a significant increase in the levels of the costimulatory molecules CD80 and CD86 on the surface of DCs in the spleen and lymph nodes of H22 mice subjected to the combined treatment (Fig. 4C and D). These results suggested that the combinatory treatment stimulated the maturation of DCs.

The combination of CUIIa and DOX remolds the immune microenvironment. To further explore whether the combination facilitated an immunoregulatory effect, the ratio of immune cells in the spleen and draining lymph nodes was measured by flow cytometry. Research has shown that $CD8^+$ T cells can be specifically activated to become tumor-specific cytotoxic lymphocytes that generate an antitumor response (32). T helper 1 cells (TH1) are the subpopulation of $CD4^+$ T helper cells that improve the immune response and enhance antitumor effects and other roles primarily through the secretion of cytokines (33,34). Although no statistical significance was observed, the percentage of splenic TH1 (IFN-γ^+CD4^+ T) cells was increased in the combination group, and exhibited the highest proportion (Fig. 5A). Both CUIIa and DOX monotherapy presented partial effect on proportion of TH1 and CTLs cells. The proportion of CTLs (IFN-γ^+CD8^+ T) cells in the spleen was significantly increased in the combined group compared with the control group. The combination treatment also increased the numbers of TH1 and CTLs cells in the draining lymph nodes (Fig. 5B). Furthermore, the combination therapy also considerably decreased the frequency of Treg cells in the spleen (Fig. 5C) and draining lymph nodes (Fig. 5D) of H22 mice.

MDSCs and M2-polarized macrophages play a central role in tumor immune evasion and tumor metastasis. Moreover, increased numbers of MDSCs and M2 macrophages are positively associated with poor prognosis and reduced survival in cancer patients (35,36). The combination therapy significantly decreased the frequencies of MDSCs in both the spleen and lymph nodes (Fig. 6A and B). In detail, there was no significant change for M-MDSCs ratio between the DOX group and

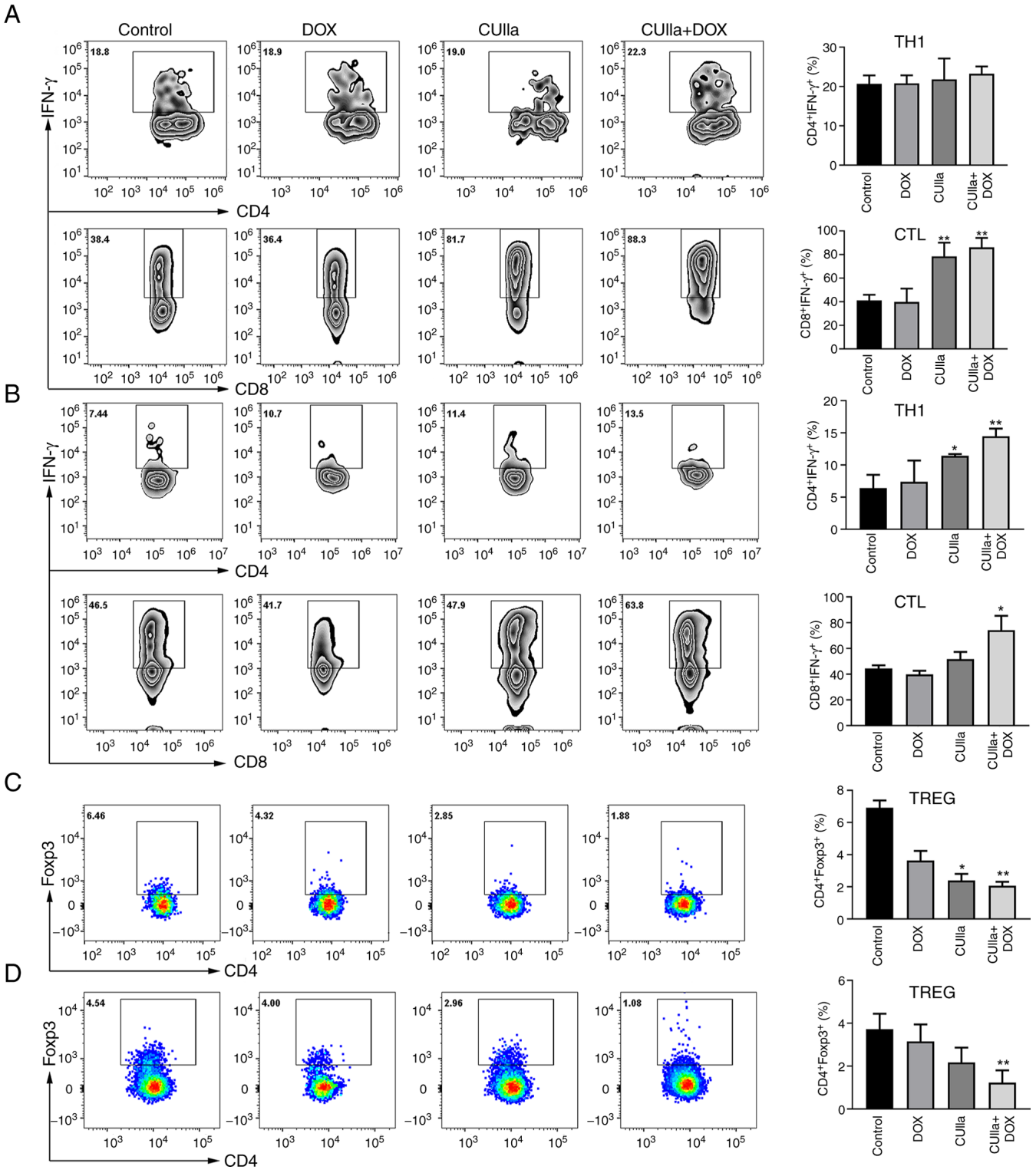

Figure 5. Changes in the immune microenvironment following combined treatment of CUIIa and DOX. (A and B) TH1 (IFN-γ$^+$CD4$^+$ T) cells and CTLs (IFN-γ$^+$CD8$^+$ T) cells in the (A) spleen and (B) draining lymph nodes of mice bearing H22 tumor. (C and D) The proportion of Treg (Foxp3$^+$CD4$^+$ T) cells in the (C) spleen and (D) draining lymph nodes of mice bearing H22 tumor. Data are presented as the mean ± SD. *P<0.05 and **P<0.01. CUIIa, cucurbitacin IIa; DOX, doxorubicin; TH1, T helper 1 cells; CTLs, cytotoxic T lymphocytes; Treg, regulatory T cells.

the control group in the spleen; however, M-MDSCs decreased significantly after the combination treatment (Fig. 6C). In the lymph nodes, single CUIIa treatment, as well as in combination with DOX, all increased the proportion of M1 macrophages and decreased the proportion of M2 polarized macrophages (Fig. 6D).

Discussion

The ICD in tumor cells is expected to provide new opportunities for immunotherapy. These ICD-inducing chemotherapy drugs can function both via the chemotherapy role and via ICD-triggered cell-eliminating immune responses, thus

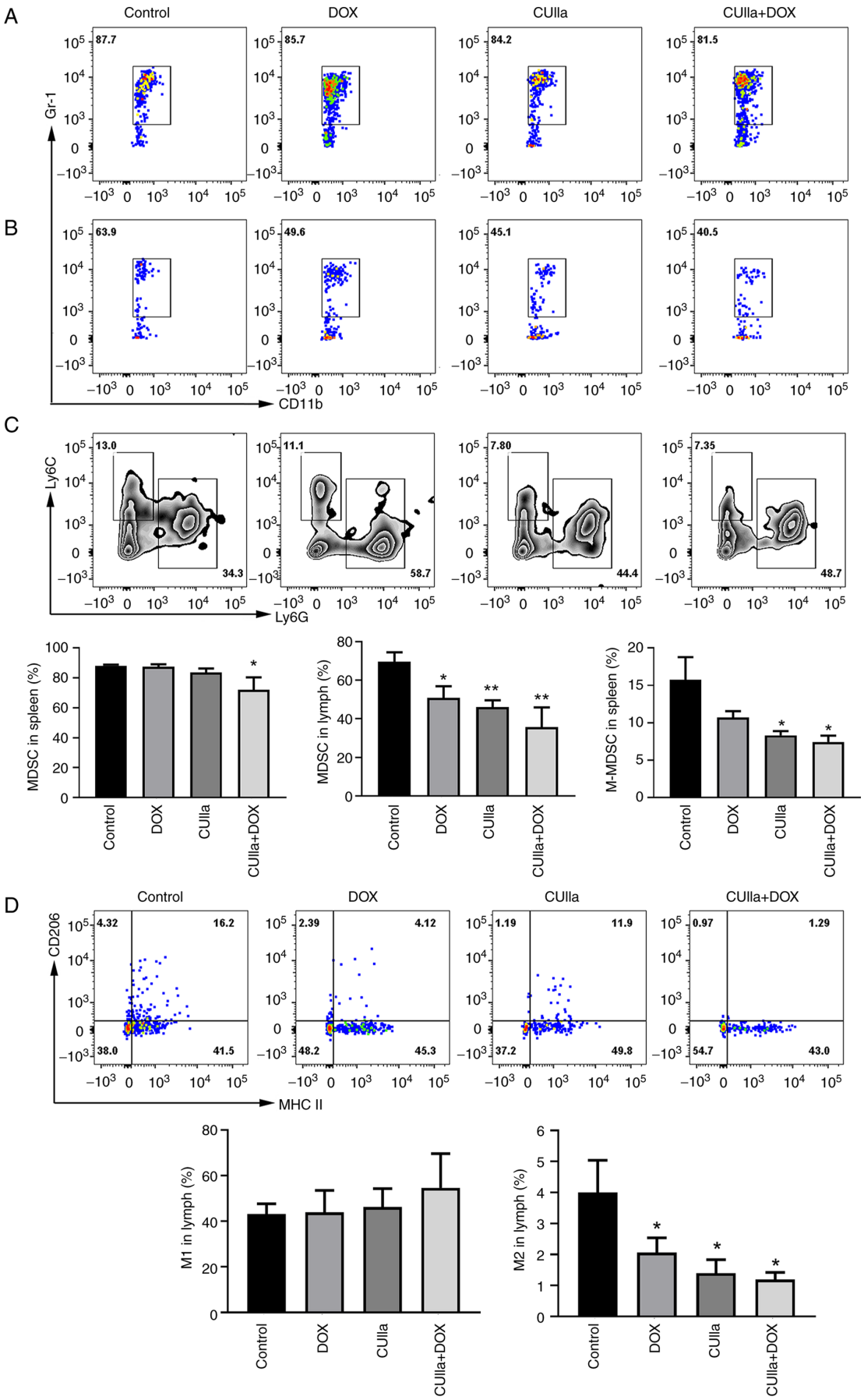

Figure 6. Combination of CUIIa and DOX decreases the proportion of MDSCs and M2 macrophages. (A and B) Representative flow cytometric plot expressing the proportion of MDSCs ($CD11b^+Gr1^+$) in the (A) spleen and (B) draining lymph nodes of mice bearing H22 tumor. (C) The proportion of monocytic MDSCs ($CD11b^+Ly6G^-Ly6C^{high}$) in the spleen. (D) The proportion of M1 ($F4/80^+MHCII^+$) and M2 ($F4/80^+CD206^+$) macrophages in draining lymph nodes. Data are presented as the mean ± SD. $^*P<0.05$ and $^{**}P<0.01$. CUIIa, cucurbitacin IIa; DOX, doxorubicin; MDSCs, myeloid-derived suppressor cells.

attaining more pleasant curative effects (3,10). However, the immunosuppressive TME and feeble antigen presentation capacity has greatly limited DOX-stimulated immune responses. In the present study, it was investigated whether CUIIa and DOX combination therapy would provoke a stronger ICD effect and reshape the immune microenvironment in liver cancer. Insights were also provided into the anticancer effects of the combination on liver cancer growth and the underlying mechanisms were explored.

The induction of apoptosis and autophagy, and cell cycle arrest have been reported to be involved in the anticancer mechanism of CUIIa (20,23,24). Consistently, CUIIa significantly inhibited the viability and colony formation of liver cancer cells in the present study. CUIIa also promoted the apoptosis of HepG2 and Hep3B cells and induced cell cycle arrest at the G2/M phase. Moreover, CUIIa considerably repressed tumor growth in H22 mice, without causing obvious damage to the major organs. Thus, CUIIa is a promising drug for the treatment of liver cancer. It is noteworthy that cucurbitacins displayed unique advantages when combined with chemotherapeutic drugs. For instance, the synergistic antitumor effects of Cucurbitacin E and Dox have been demonstrated on gastric cancer both *in vitro* and *in vivo* (37). Cucurbitacin B enhanced the inhibition ability of cisplatin on resistant ovarian cancer cells, and played an important role in eliciting antitumor immunity (38). In the present study, as expected, the IC_{50} of DOX on HepG2 cells was significantly decreased after the co-administration with CUIIa. Particularly, the strongest antitumor effect was attained when the molar ratio of CUIIa to DOX was 10:1. Hoechst staining and flow cytometric analysis also verified that CUIIa promoted DOX-induced apoptosis in HepG2 cells. Mice bearing H22 subcutaneous xenograft were used to evaluate the combined effect of CUIIa and DOX *in vivo*. The combination group significantly inhibited tumor growth and the expression of Ki67 and CD31 in mice. More importantly, DOX-induced myocardial toxicity was alleviated after combinatory treatment. Therefore, the combined administration can bring down the dosage of DOX chemotherapy while simultaneously ensuring an anticancer effect at the same time, inferring that CUIIa might potentially function as a chemotherapy adjuvant in treating liver cancer.

Notably, DOX can also stimulate ICD and thus triggering an immune response, although the immunogenicity induced by DOX is not strong enough to eliminate cancer cells. It was found that CUIIa promoted DOX-induced apoptosis and that ICD was caspase-dependent. The upregulation of various DAMPs can serve as markers of ICD occurrence. Therefore, expression of DAMPs was next detected to examine whether the combination of CUIIa and DOX could reinforce ICD. During the ICD process, CRT is exposed on the membrane of dying cells, which is considered as an 'Eat Me' signal, attracting and activating DCs (39). HMGB1 is released from the nucleus during the late stages of apoptosis, promoting chemotaxis of DCs and antigen presentation to T cells (40,41). ATP, which acts as a find-me signal, induces migration of DCs to tumor cells (42). In the present study, the combination of CUIIa and DOX induced ICD with the upregulation of various DAMPs, indicating that when combined with CUIIa, DOX provokes a satisfactory ICD effect, even at a low dose.

In the liver cancer microenvironment, the inflammatory cell infiltrate is unbalanced towards an immunosuppressive phenotype, with a prevalence of Tregs, regulatory B cells (Bregs), M2 macrophages and MDSCs, over M1 macrophages, DCs, TH1 and CTLs. DAMPs excreted by dying cells can initiate an immune response, followed by the maturation of the antigen-presenting DCs. However, the immunosuppressive TME hinders the anticancer immune response triggered by DCs (43). MDSCs, Tregs and tumor cells secrete suppressive cytokines, that can inhibit CTLs (44,45). Bregs were shown to facilitate liver cancer progression by promoting IL-10 and TGF-β secretion. Bregs cells also inhibit T cell antitumor immune response by converting naive $CD4^+$ T cells to Treg cells in the TME (46). Accumulation of monocytic MDSCs (M-MDSCs) in fibrotic livers is meaningfully associated with abridged tumor-infiltrating lymphocytes and amplified tumorigenicity in mice (47). Hormone divergences play an important part in modifying the TME. In the future precision therapies, gender-specific medicine will become a significant modality. As male-female differences might affect the TME (48), only male mice were chosen for the present study. It was found that CUIIa combined with DOX improved the immune microenvironment of mice bearing H22 tumor. Immuno-surveillance cells including TH1, CTLs, M1 macrophages and activated DCs, increased, whereas the number of immunosuppressive cells, including M2 macrophages, Tregs, MDSCs and M-MDSCs, declined. Concerning the important role of Bregs in liver cancer progression, the role of Bregs in DOX-induced ICD will be evaluated in the authors' future studies.

CUIIa has been reported to increase levels of LC3-II conjugates and formation of LC3 puncta of RAW 264.7 cells, suggesting that autophagy can be triggered by CUIIa (49). Autophagy was regarded as an inducer of ICD. DAMPs released by dying cells including autophagic cells bind to the receptor on phagocytic cells and subsequently trigger an immune response (19). It was assumed that CUIIa enhanced DOX-induced ICD via triggering autophagy, and it was found that CUIIa promoted LC3 expression in HCC cells (data not shown). To verify the hypothesis and explore the specific mechanism by which CUIIa enhances DOX-induced ICD, more profound work needs be performed in the future such as colocalization of autophagosome and mitochondria, and expression of mitophagy biomarkers. Moreover, Bafilomycin A1, an autophagy inhibitor, will be used to verify the association of autophagy and ATP release.

In conclusion, the present findings demonstrated the capability of CUIIa to potentiate the anticancer effect of DOX in liver cancer, probably by inducing apoptosis and ICD, as well as by reprogramming the immune microenvironment. This suggested the feasibility and safety of using CUIIa as an adjuvant drug for DOX in liver cancer therapy to improve therapy responsiveness, reduce unwanted cardiotoxicity, and overcome the adverse effects of the TME.

Acknowledgements

Not applicable.

Funding

The present study was supported by the National Natural Science Foundation of China (grant no. 81873055), the Jiangsu Clinical Innovation Center of Digestive Cancer of Traditional

Chinese Medicine (grant no. 2021.6), the Jiangsu Traditional Chinese Medicine Development Plan Project (grant no. MS2023033) and the Jiangsu Provincial Association for Maternal and Child Health Studies (grant no. JSFY202202).

Availability of data and materials

The datasets used and/or analyzed during the current study are available from the corresponding author on reasonable request.

Authors' contributions

SJL and SW carried out the experiment and wrote the first draft of the manuscript. SJL, GLW and SW designed the experiment. LXL, JS, APZ and GLW analyzed the data. ZJF interpreted the data and revised the manuscript. ZJF and GLW gave the final approval and supervised the project. All authors read and approved the final manuscript. SJL and GLW confirm the authenticity of all the raw data.

Ethics approval and consent to participate

All mice experiments were approved by the Institutional Animal Care and Use Committee of the Jiangsu Academy of Chinese Medicine (approval no. AEWC-20220505-203; Nanjing, China). All animal experiments complied with the ARRIVE guidelines, the U.K. Animals (Scientific Procedures) Act, 1986, as well as the National Research Council's Guide for the Care and Use of Laboratory Animals. Great effort was made to decrease the pain and number of animals.

Patient consent for publication

Not applicable.

Competing interests

The authors declare that they have no competing interests.

References

1. Huang J, Hao P, Zhang YL, Deng FX, Deng Q, Hong Y, Wang XW, Wang Y, Li TT, Zhang XG, *et al*: Discovering multiple transcripts of human hepatocytes using massively parallel signature sequencing (MPSS). BMC Genomics 8: 207, 2007.
2. Plaz Torres MC, Bodini G, Furnari M, Marabotto E, Zentilin P, Strazzabosco M and Giannini EG: Surveillance for hepatocellular carcinoma in patients with non-alcoholic fatty liver disease: universal or selective? Cancers (Basel) 12: 1422, 2020.
3. He T, Wang L, Gou S, Lu L, Liu G, Wang K, Yang Y, Duan Q, Geng W, Zhao P, *et al*: Enhanced immunogenic cell death and antigen presentation via engineered bifidobacterium bifidum to boost chemo-immunotherapy. ACS Nano 17: 9953-9971, 2023.
4. Lu Q, Huang H, Wang X, Luo L, Xia H, Zhang L, Xu J, Huang Y, Luo X and Luo J: Echinatin inhibits the growth and metastasis of human osteosarcoma cells through Wnt/β-catenin and p38 signaling pathways. Pharmacol Res 191: 106760, 2023.
5. Vanmeerbeek I, Sprooten J, De Ruysscher D, Tejpar S, Vandenberghe P, Fucikova J, Spisek R, Zitvogel L, Kroemer G, Galluzzi L, *et al*: Trial watch: Chemotherapy-induced immunogenic cell death in immuno-oncology. Oncoimmunology 9: 1703449, 2020.
6. Obeid M, Tesniere A, Ghiringhelli F, Fimia GM, Apetoh L, Perfettini JL, Castedo M, Mignot G, Panaretakis T, Casares N, *et al*: Calreticulin exposure dictates the immunogenicity of cancer cell death. Nat Med 13: 54-61, 2007.
7. Green DR, Ferguson T, Zitvogel L and Kroemer G: Immunogenic and tolerogenic cell death. Nat Rev Immunol 9: 353-363, 2009.
8. Casares N, Pequignot MO, Tesniere A, Ghiringhelli F, Roux S, Chaput N, Schmitt E, Hamai A, Hervas-Stubbs S, Obeid M, *et al*: Caspase-dependent immunogenicity of doxorubicin-induced tumor cell death. J Exp Med 202: 1691-1701, 2005.
9. Birmpilis AI, Paschalis A, Mourkakis A, Christodoulou P, Kostopoulos IV, Antimissari E, Terzoudi G, Georgakilas AG, Armpilia C, Papageorgis P, *et al*: Immunogenic cell death, DAMPs and prothymosin α as a putative anticancer immune response biomarker. Cells 11: 1415, 2022.
10. Zhai J, Gu X, Liu Y, Hu Y, Jiang Y and Zhang Z: Chemotherapeutic and targeted drugs-induced immunogenic cell death in cancer models and antitumor therapy: An update review. Front Pharmacol 14: 1152934, 2023.
11. Shi Y, Hou X, Yu S, Pan X, Yang M, Hu J and Wang X: Targeted delivery of doxorubicin into tumor cells to decrease the in vivo toxicity of glutathione-sensitive prodrug-poloxamer188-b-poly-caprolactone nanoparticles and improve their anti-tumor activities. Colloids Surf B Biointerfaces 220: 112874, 2022.
12. Wu PJ, Chiou HL, Hsieh YH, Lin CL, Lee HL, Liu IC and Ying TH: Induction of immunogenic cell death effect of licoricidin in cervical cancer cells by enhancing endoplasmic reticulum stress-mediated high mobility group box 1 expression. Environ Toxicol 38: 1641-1650, 2023.
13. Aria H and Rezaei M: Immunogenic cell death inducer peptides: A new approach for cancer therapy, current status and future perspectives. Biomed Pharmacother 161: 114503, 2023.
14. Lu Y, Sun W, Du J, Fan J and Peng X: Immuno-photodynamic therapy (IPDT): Organic photosensitizers and their application in cancer ablation. JACS Au 3: 682-699, 2023.
15. Shimabukuro-Vornhagen A, Draube A, Liebig TM, Rothe A, Kochanek M and von Bergwelt-Baildon MS: The immunosuppressive factors IL-10, TGF-β, and VEGF do not affect the antigen-presenting function of CD40-activated B cells. J Exp Clin Cancer Res 31: 47, 2012.
16. Fan X, Jin J, Yan L, Liu L, Li Q and Xu Y: The impaired anti-tumoral effect of immune surveillance cells in the immune microenvironment of gastric cancer. Clin Immunol 219: 108551, 2020.
17. Dai Z, Tang J, Gu Z, Wang Y, Yang Y, Yang Y and Yu C: Eliciting immunogenic cell death via a unitized nanoinducer. Nano Lett 20: 6246-6254, 2020.
18. Wu H, Wei G, Luo L, Li L, Gao Y, Tan X, Wang S, Chang H, Liu Y, Wei Y, *et al*: Ginsenoside Rg3 nanoparticles with permeation enhancing based chitosan derivatives were encapsulated with doxorubicin by thermosensitive hydrogel and anti-cancer evaluation of peritumoral hydrogel injection combined with PD-L1 antibody. Biomater Res 26: 77, 2022.
19. Yu Z, Guo J, Hu M, Gao Y and Huang L: Icaritin exacerbates mitophagy and synergizes with doxorubicin to induce immunogenic cell death in hepatocellular carcinoma. ACS Nano 14: 4816-4828, 2020.
20. Zeng Y, Wang J, Huang Q, Ren Y, Li T, Zhang X, Yao R and Sun J: Cucurbitacin IIa: A review of phytochemistry and pharmacology. Phytother Res 35: 4155-4170, 2021.
21. Peng Y, Chen T, Luo L, Li L, Cao W, Xu X, Zhang Y, Yue P, Dai X, Ji Z, *et al*: Isoforskolin and cucurbitacin IIa promote the expression of anti-inflammatory regulatory factor SIGIRR in human macrophages stimulated with Borrelia burgdorferi basic membrane protein A. Int Immunopharmacol 88: 106914, 2020.
22. Singh N, Krishnakumar S, Kanwar RK, Cheung CH and Kanwar JR: Clinical aspects for survivin: A crucial molecule for targeting drug-resistant cancers. Drug Discov Today 20: 578-587, 2015.
23. Zhang J, Song Y, Liang Y, Zou H, Zuo P, Yan M, Jing S, Li T, Wang Y, Li D, *et al*: Cucurbitacin IIa interferes with EGFR-MAPK signaling pathway leads to proliferation inhibition in A549 cells. Food Chem Toxicol 132: 110654, 2019.
24. Boykin C, Zhang G, Chen YH, Zhang RW, Fan XE, Yang WM and Lu Q: Cucurbitacin IIa: a novel class of anti-cancer drug inducing non-reversible actin aggregation and inhibiting survivin independent of JAK2/STAT3 phosphorylation. Br J Cancer 104: 781-789, 2011.
25. Yu K, Yang X, Li Y, Cui X, Liu B and Yao Q: Synthesis of cucurbitacin IIa derivatives with apoptosis-inducing capabilities in human cancer cells. RSC Adv 10: 3872-3881, 2020.
26. Kuang Z, Wu J, Tan Y, Zhu G, Li J and Wu M: MicroRNA in the diagnosis and treatment of doxorubicin-induced cardiotoxicity. Biomolecules 13: 568, 2023.

27. Yu S, Cai X, Wu C, Liu Y, Zhang J, Gong X, Wang X, Wu X, Zhu T, Mo L, *et al*: Targeting HSP90-HDAC6 regulating network implicates precision treatment of breast cancer. Int J Biol Sci 13: 505-517, 2017.
28. O'Donohue TJ, Ibáñez G, Coutinho DF, Mauguen A, Siddiquee A, Rosales N, Calder P, Ndengu A, You D, Long M, *et al*: Translational strategies for repotrectinib in neuroblastoma. Mol Cancer Ther 20: 2189-2197, 2021.
29. Bhagat A and Kleinerman ES: Anthracycline-induced cardiotoxicity: Causes, mechanisms, and prevention. Adv Exp Med Biol 1257: 181-192, 2020.
30. Ma X, Yang S, Zhang T, Wang S, Yang Q, Xiao Y, Shi X, Xue P, Kang Y, Liu G, *et al*: Bioresponsive immune-booster-based prodrug nanogel for cancer immunotherapy. Acta Pharm Sin B 12: 451-466, 2022.
31. Bao L, Hao C, Wang J, Wang D, Zhao Y, Li Y and Yao W: High-dose cyclophosphamide administration orchestrates phenotypic and functional alterations of immature dendritic cells and regulates Th cell polarization. Front Pharmacol 11: 775, 2020.
32. Shan Z, Wang H, Zhang Y and Min W: The role of tumor-derived exosomes in the abscopal effect and immunotherapy. Life (Basel) 11: 381, 2021.
33. Deng Z, Zhang M, Zhu T, Zhili N, Liu Z, Xiang R, Zhang W and Xu Y: Dynamic changes in peripheral blood lymphocyte subsets in adult patients with COVID-19. Int J Infect Dis 98: 353-358, 2020.
34. Yu H, Zou W, Mi C, Wang Q, Dai G, Zhang T, Zhang G, Xie K, Wang J and Shi H: Research Note: Expression of T cell-related cytokines in chicken cecal and spleen tissues following Eimeria tenella infection in vivo. Poult Sci 100: 101161, 2021.
35. Sasidharan Nair V, Saleh R, Toor SM, Taha RZ, Ahmed AA, Kurer MA, Murshed K, Alajez NM, Abu Nada M and Elkord E: Transcriptomic profiling disclosed the role of DNA methylation and histone modifications in tumor-infiltrating myeloid-derived suppressor cell subsets in colorectal cancer. Clin Epigenetics 12: 13, 2020.
36. Wellenstein MD and de Visser KE: Cancer-cell-intrinsic mechanisms shaping the tumor immune landscape. Immunity 48: 399-416, 2018.
37. Si W, Lyu J, Liu Z, Wang C, Huang J, Jiang L and Ma T: Cucurbitacin E inhibits cellular proliferation and enhances the chemo-response in gastric cancer by suppressing AKt activation. J Cancer 10: 5843-5851, 2019.
38. Yin S, Mai Z, Liu C, Xu L and Xia C: Label-free-based quantitative proteomic analysis of the inhibition of cisplatin-resistant ovarian cancer cell proliferation by cucurbitacin B. Phytomedicine 111: 154669, 2023.
39. Ni K, Lan G, Guo N, Culbert A, Luo T, Wu T, Weichselbaum RR and Lin W: Nanoscale metal-organic frameworks for x-ray activated in situ cancer vaccination. Sci Adv 6: eabb5223, 2020.
40. Sun D, Zou Y, Song L, Han S, Yang H, Chu D, Dai Y, Ma J, O'Driscoll CM, Yu Z and Guo J: A cyclodextrin-based nanoformulation achieves co-delivery of ginsenoside Rg3 and quercetin for chemo-immunotherapy in colorectal cancer. Acta Pharm Sin B 12: 378-393, 2022.
41. Yang Q, Shi G, Chen X, Lin Y, Cheng L, Jiang Q, Yan X, Jiang M, Li Y, Zhang H, *et al*: Nanomicelle protects the immune activation effects of Paclitaxel and sensitizes tumors to anti-PD-1 immunotherapy. Theranostics 10: 8382-8399, 2020.
42. Wu Q, Li B, Li J, Sun S, Yuan J and Sun S: Cancer-associated adipocytes as immunomodulators in cancer. Biomark Res 9: 2, 2021.
43. Szczygieł A, Węgierek-Ciura K, Wróblewska A, Mierzejewska J, Rossowska J, Szermer-Olearnik B, Świtalska M, Anger-Góra N, Goszczyński TM and Pajtasz-Piasecka E: Combined therapy with methotrexate nanoconjugate and dendritic cells with downregulated IL-10R expression modulates the tumor microenvironment and enhances the systemic anti-tumor immune response in MC38 murine colon carcinoma. Front Immunol 14: 1155377, 2023.
44. Evgin L and Vile RG: Parking CAR T cells in tumours: Oncolytic viruses as valets or vandals? Cancers (Basel) 13: 1106, 2021.
45. Li J, Zhao M, Liang W, Wu S, Wang Z and Wang D: Codelivery of Shikonin and siTGF-β for enhanced triple negative breast cancer chemo-immunotherapy. J Control Release 342: 308-320, 2022.
46. Shao Y, Lo CM, Ling CC, Liu XB, Ng KTP, Chu ACY, Ma YY, Li CX, Fan ST and Man K: Regulatory B cells accelerate hepatocellular carcinoma progression via CD40/CD154 signaling pathway. Cancer Lett 355: 264-272, 2014.
47. Liu M, Zhou J, Liu X, Feng Y, Yang W, Wu F, Cheung OKW, Sun H, Zeng X, Tang W, *et al*: Targeting monocyte-intrinsic enhancer reprogramming improves immunotherapy efficacy in hepatocellular carcinoma. Gut 69: 365-379, 2020.
48. He F, Furones AR, Landegren N, Fuxe J and Sarhan D: Sex dimorphism in the tumor microenvironment-from bench to bedside and back. Semin Cancer Biol 86: 166-179, 2022.
49. He J, Wang Y, Xu LH, Qiao J, Ouyang DY and He XH: Cucurbitacin IIa induces caspase-3-dependent apoptosis and enhances autophagy in lipopolysaccharide-stimulated RAW 264.7 macrophages. Int Immunopharmacol 16: 27-34, 2013.